

Available at www.sciencedirect.comjournal homepage: www.elsevier.com/locate/he

Synthesis and characterization of $\text{BaIn}_{0.3-x}\text{Y}_x\text{Ce}_{0.7}\text{O}_{3-\delta}$ ($x = 0, 0.1, 0.2, 0.3$) proton conductors

Fei Zhao^a, Qiang Liu^a, Siwei Wang^a, Kyle Brinkman^b, Fanglin Chen^{a,*}

^a Department of Mechanical Engineering, University of South Carolina, Columbia, SC 29208, USA

^b Savannah River National Laboratory, Aiken, SC 29808, USA

ARTICLE INFO

Article history:

Received 15 January 2010

Received in revised form

10 February 2010

Accepted 13 February 2010

Available online 20 March 2010

Keywords:

Barium cerate

Proton conductor

Electrical property

Stability

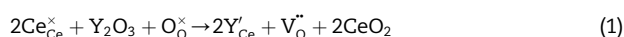
ABSTRACT

The morphological and electrical properties of yttrium (Y) and indium (In) doped barium cerate perovskites of the form $\text{BaIn}_{0.3-x}\text{Y}_x\text{Ce}_{0.7}\text{O}_{3-\delta}$ (with $x = 0-0.3$) prepared by a modified Pechini method were investigated as potential high temperature proton conductors with improved chemical stability and conductivity. The sinterability increased with the increase of In-doping, and the perovskite phase was found in the $\text{BaIn}_{0.3-x}\text{Y}_x\text{Ce}_{0.7}\text{O}_{3-\delta}$ solid solutions over the range $0 \leq x \leq 0.3$. The conductivities decreased from $x = 0.3$ to 0 while the tolerance to wet CO_2 improved for $\text{BaIn}_{0.3-x}\text{Y}_x\text{Ce}_{0.7}\text{O}_{3-\delta}$ samples with an increase of In-doping. $\text{BaIn}_{0.1}\text{Y}_{0.2}\text{Ce}_{0.7}\text{O}_{3-\delta}$ was found to have relatively high conductivity as well as acceptable wet CO_2 stability.

© 2010 Professor T. Nejat Veziroglu. Published by Elsevier Ltd. All rights reserved.

1. Introduction

In the past two decades, high temperature proton conductors with the ABO_3 perovskite structure, such as BaCeO_3 , BaZrO_3 , SrCeO_3 and SrZrO_3 have been extensively studied due to the low activation energy and high proton conductivity [1–4]. Among them, doped barium cerates, $\text{BaCe}_{1-x}\text{A}_x\text{O}_{3-\delta}$ ($\text{A} = \text{Y}^{3+}$, In^{3+} , rare-earth ions such as Nd^{3+} , Sm^{3+} , Gd^{3+} , Eu^{3+} and Yb^{3+}) have exhibited particularly high proton conductivity [5–11]. In general, the highest proton conductivity among the barium cerates and zirconates has been observed with Y^{3+} doping, followed by Gd^{3+} and other lanthanides [3,12,13]. The increase in proton conductivity with doping is mainly related to the formation of protonic defects in the ABO_3 perovskites due to dissociative adsorption of water in the presence of oxygen vacancies. In the case of Y-doped BaCeO_3 , the creation of oxygen vacancies through the defect reaction can be written in the Kroger–Vink notation as:



where $\text{Ce}_{\text{Ce}}^{\times}$ and $\text{O}_{\text{O}}^{\times}$ are lattice cerium ions and lattice oxygen ions, respectively. Y'_{Ce} denotes yttrium ion occupied at cerium ion site. The formation of hydroxyl ions (OH'_{O}) with oxygen vacancies ($\text{V}_{\text{O}}^{\bullet\bullet}$) takes place on the oxygen-ion site for the incorporation of water through:



The mechanism of proton migration by a series of jumps from one position to the next position in perovskite oxides was proposed by Iwahara [13] and further analyzed by Kreuer [12]. Oxygen vacancies are the main defects at high temperatures where water molecule desorption takes place, together with oxygen migration in the bulk while the dissolution of protons is favoured by decreasing temperatures. The proton conduction becomes predominate at intermediate temperatures near 600 °C.

* Corresponding author. Tel.: +1 803 777 4785.

E-mail address: chenfa@cec.sc.edu (F. Chen).

0360-3199/\$ – see front matter © 2010 Professor T. Nejat Veziroglu. Published by Elsevier Ltd. All rights reserved.

doi:10.1016/j.ijhydene.2010.02.080

High temperature proton conductors have a wide range of applications. Firstly, they can be used as electrolytes for solid oxide fuel cells (SOFCs) [1]. SOFC is an energy conversion device that directly produces electricity by electrochemical combination of a fuel and an oxidant with high efficiency and extremely low to zero emissions [1]. They can also be used as membranes for hydrogen separation, enabling the production of high purity hydrogen from coal gasified gas streams [14]. Hydrogen is an attractive fuel for both the electric power and transportation industries due to carbon free combustion products which address rising concerns over the global climate change. In addition, high temperature proton conductors may play an important role in the next generation nuclear power plant since they can be used to isolate hydrogen isotope contaminants present in the helium gas streams utilized for reactor cooling [15]. In all of the above applications, high proton conductivity and good chemical stability are required to enhance the device performance.

Although Y-doped BaCeO₃ possesses the highest proton conductivity among all perovskite-type high temperature proton conducting oxides studied so far, barium cerates can easily decompose into barium carbonate and/or barium hydroxide, and cerium oxide at elevated temperatures in CO₂ and/or in humid atmospheres. Consequently, recent works have been focused on the development and optimization of the performance of doped cerates in order to enhance their chemical stabilities without remarkably sacrificing their proton conductivities [12,16,17]. Among the different strategies exploited, the most popular approach is to prepare mixed barium cerate/barium zirconate solid solution. Although zirconate-based proton conductors are relatively more stable at elevated temperatures in CO₂ and or in humid atmospheres, they have much lower conductivity. BaCeO₃ and BaZrO₃ can easily form a solid solution across the entire composition range. Consequently, it might be possible to replace a fraction of Ce in BaCeO₃ with Zr, thereby achieving a solid solution of cerate and zirconate with both good protonic conductivity and chemical stability. Further it has been recently reported that a Zr-free barium cerate (i.e. In-doped BaCeO₃) possesses good stability at elevated temperatures in CO₂ and H₂O-rich environments [18,19]. However, the electrical conductivity of In-doped BaCeO₃ proton conductors is relatively low [6,20]. To improve the conductivity of In-doped BaCeO₃ proton conductor, yttria could be used as co-dopant since yttria doped BaCeO₃ has high conductivity among doped BaCeO₃. The same strategy of “co-doping” has been successfully applied on BaCe_{0.8-x}M_xY_{0.2}O_{3-δ} with M (M = Ta, Ti, and Sn) and Y as the co-dopants and proved to maintain both high conductivity and good stability [21–23]. Consequently, it is anticipated that co-doping the B-site with In and Y while maintaining high Ce content (e.g., 0.7) might offer a unique composition with elevated proton conductivity and improved stability in CO₂ and H₂O-rich environments. In this work, BaIn_{0.3-x}Y_xCe_{0.7}O_{3-δ} (BIYC, x = 0, 0.1, 0.2, 0.3) solid solutions prepared by a modified Pechini method has been investigated to find a composition having both high conductivity and good stability.

2. Experimental

2.1. Fabrication of perovskite powders

Powder samples of barium cerate solid solutions having the nominal composition of BaIn_{0.3-x}Y_xCe_{0.7}O_{3-δ} (x = 0, 0.1, 0.2, 0.3) were synthesized by a sol-gel modified Pechini process to ensure good homogeneity of the mixed oxides. The starting materials were Ba(NO₃)₂ (Alfa Aesar, 99.95%), Ce(NO₃)₃·6H₂O (Alfa Aesar, 99.5%), In(NO₃)₃·4.7H₂O (Alfa Aesar, In 29% min), and Y(NO₃)₃·6H₂O (Alfa Aesar, 99.9%) as metal precursors and EDTA (Ethylenediaminetetraacetic acid, Alfa Aesar, 99%) and citric acid (Alfa Aesar, 99%) as chelating and complexing agents, respectively. The water content of the indium salt was determined by thermogravimetric analysis. Ammonium hydroxide (Sigma-Aldrich, NH₃ content 28.0–30.0%) was added to promote the dissolution of EDTA in deionized water. An appropriate amount of barium nitrate was first dissolved in deionized water. Following that, an aqueous solution of EDTA and ammonia (pH ~ 9) was added drop wise to the barium solution. The mixture was kept at 50 °C with mild continuous stirring until a clear solution was obtained. An aqueous solution containing stoichiometric amounts of cerium, indium and yttrium salts was subsequently slowly added to the barium nitrate solution. Finally, an appropriate amount of citric acid was added (citric acid:metal nitrates:EDTA molar ratios = 1.5:1:1) and the final solution was stirred at room temperature for 24 h. Water was then slowly evaporated on a hot plate and the resulting brown gel was dried at 300 °C. The dried ashes were then heat-treated at 600 °C in air for 2 h (heating rate 3 °C min⁻¹) to remove the organic residue. The temperature of the thermal treatment was chosen based upon thermogravimetric analyses performed on the as-prepared precursor with flowing air. Fine BaIn_{0.3-x}Y_xCe_{0.7}O_{3-δ} powders were obtained by calcination the heat-treated powders at 1000 °C in air for 6 h (heating rate 3 °C min⁻¹).

2.2. Characterization of the proton conductor

The resulting fine powders were uni-axially pressed into pellets at 400 MPa. The pellets were sintered at 1450 °C for 5 h in air and the crystalline structure of the sintered samples was measured using an X-ray powder diffractometer (Mini X-ray diffractometer with graphite-monochromatized CuK_α radiation (λ = 1.5418 Å)), employing a scanning rate of 10° min⁻¹ in the 2θ range of 20–80°. Densification studies were performed by direct measurements of sample weight and dimensions after linear shrinkage due to sintering. Morphological investigations on the prepared powder and sintered disks were based on the scanning electron microscopy (SEM) observations using a FEI Quanta (XL 30 model). For conductivity measurement, both sides of the sintered disks were polished with 400 grade SiC sandpaper and then cleaned in an ultrasonic cleaner. Platinum paste (Heraeus, component metallization CL11-5349) was painted on both sides of the samples, and then heat-treated at 1000 °C for 1 h to form a porous platinum electrode. Platinum wires were attached to the surface of pellet. Electrical conductivity was measured by A.C.

impedance method. A.C. impedance responses were collected with the A.C. amplitude of 10 mV in the frequency range between 0.01 Hz and 1 MHz using an electrochemical station (Metek, Versa STAT3-400) in different atmospheres at 500–800 °C (50 °C per step). From the intercepts of impedance plots with the real axis, the ohmic resistance of the samples can be determined. The total conductivity is obtained using the following equation: $\sigma = L/(RS)$, where σ is the conductivity in unit of $(\Omega \text{ cm})^{-1}$, L is the sample thickness in unit of cm, R is the ohmic resistance in unit of Ω and S is the Pt electrode area in unit of cm^2 .

3. Results and discussion

3.1. Perovskite phase formation

Fig. 1 shows the XRD data for $\text{BaIn}_{0.3-x}\text{Y}_x\text{Ce}_{0.7}\text{O}_{3-\delta}$ as a function of the Y content. A single phase perovskite structure was obtained for most of these compositions. For the In-doped materials, $\text{BaIn}_{0.3}\text{Ce}_{0.7}\text{O}_{3-\delta}$ was determined to be an orthorhombic $Pm\bar{c}n$ unit cell even when the In^{3+} content was increased up to 30%, as reported by Giannici [24]. However, for the Y-doped barium cerate, the Y dopant solubility limit is less than 20% of the available Ce sites. Consequently, the Y_2O_3 phase segregated at the grain boundaries in $\text{BaY}_{0.3}\text{Ce}_{0.7}\text{O}_{3-\delta}$, as can be seen from the XRD pattern in Fig. 1. In^{3+} and Y^{3+} have effective ionic radii of 0.80 Å and 0.90 Å, respectively, implying that the doping of Y^{3+} should lead to an increase in lattice parameters. This was confirmed by the XRD peaks for the samples where higher Y doping resulted in slight peak shift toward lower 2θ , indicating an increase in the lattice parameter. In addition, it was observed that Y^{3+} adapts poorly to insertion in the host lattices in cerate due to its very high hardness. On the other hand, In^{3+} , being much softer than Y^{3+} (i.e., more easily polarized), can be more effectively inserted in the host lattices since its low hardness allows for the release of the resulting strain and consequently stabilizes the structure [24].

3.2. Sinterability of the proton conductor

To investigate the sinterability of the In-doped powders, morphologies of the powders and sintered ceramics were

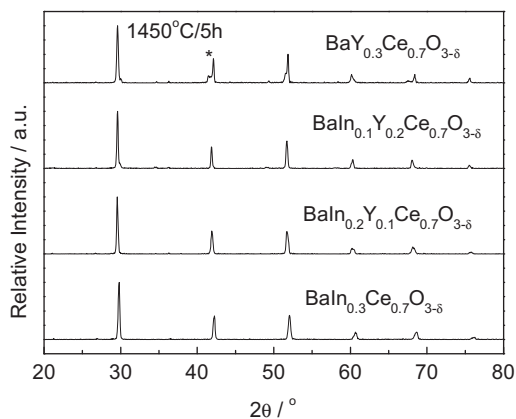


Fig. 1 – XRD patterns of $\text{BaIn}_{0.3-x}\text{Y}_x\text{Ce}_{0.7}\text{O}_{3-\delta}$ ($x = 0, 0.1, 0.2, 0.3$) samples sintered at 1450 °C for 5 h in air. *: Y_2O_3 .

analyzed by SEM. As shown in Fig. 2, the SEM image of the $\text{BaIn}_{0.3}\text{Ce}_{0.7}\text{O}_{3-\delta}$ powder calcined at 1000 °C for 6 h in air reveals a network-like morphology with plenty of voids distributed inside a foam-like structure. The morphologies for the other BICY powders with different compositions are similar. Such fluffy powders having very low filled density are particularly suitable for fabricating thin membranes by a dry-pressing method [25]. After sintering the BIYC pellets at 1450 °C for 5 h, the size of crystalline grains and the number of closed pores increase with Y doping content as shown from the cross-sectional views of those ceramic disks in Fig. 3. The average grain size is determined using a linear intercept method by counting the adjacent grains in the SEM graphs. The average grain sizes are 5.6, 8.5, 12.7 and 15.2 μm for $\text{BaIn}_{0.3-x}\text{Y}_x\text{Ce}_{0.7}\text{O}_{3-\delta}$ ($x = 0, 0.1, 0.2, 0.3$) samples, respectively. The sintering conditions used in this work are normally employed in fabricating BaCeO_3 -based SOFCs. Of course, from the results in this study it may be expected that high densities of the BIYC samples might be achieved at relatively lower sintering temperature or for shorter dwell time. Further work is needed in order to study when and how the grain growth happens and what the effects of the grain size on chemical stability and conductivity of the sintered BIYC samples. The packing between $\text{BaIn}_{0.3}\text{Ce}_{0.7}\text{O}_{3-\delta}$ crystallites is more compact than that of $\text{BaY}_{0.3}\text{CeO}_3$, which is consistent with the shrinkage results of those sintered pellets. After sintering at 1450 °C for 5 h, the linear shrinkages of the disk diameters are 12.3%, 12.0%, 11.5% and 10.3% for $\text{BaIn}_{0.3-x}\text{Y}_x\text{Ce}_{0.7}\text{O}_{3-\delta}$ ($x = 0, 0.1, 0.2, 0.3$) samples, respectively. The results of Archimedes's water displacement measurements on the sintered disks showed that all the BIYC sintered samples have relative densities greater than 94% of the theoretic values (e.g. $\text{BaIn}_{0.2}\text{Y}_{0.1}\text{Ce}_{0.7}\text{O}_{3-\delta}$ has a theoretical density of 6.351 g/cm^3). Consequently, In-doping results in an improved sinterability of BIYC.

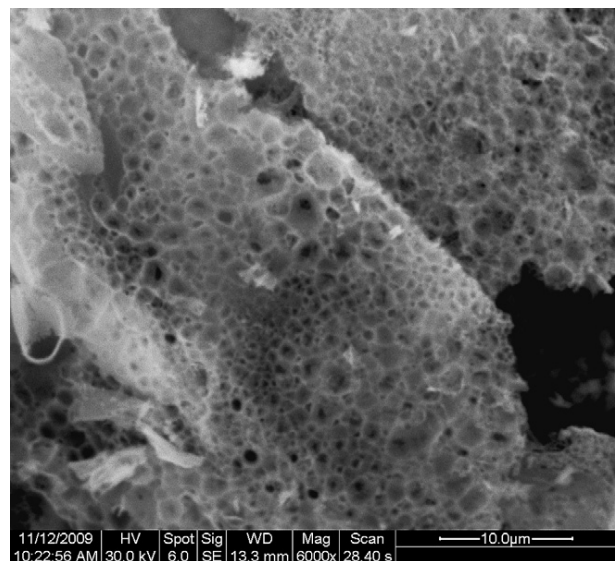


Fig. 2 – SEM photograph of $\text{BaIn}_{0.3}\text{Ce}_{0.7}\text{O}_{3-\delta}$ powder sintered at 1000 °C for 6 h in air.

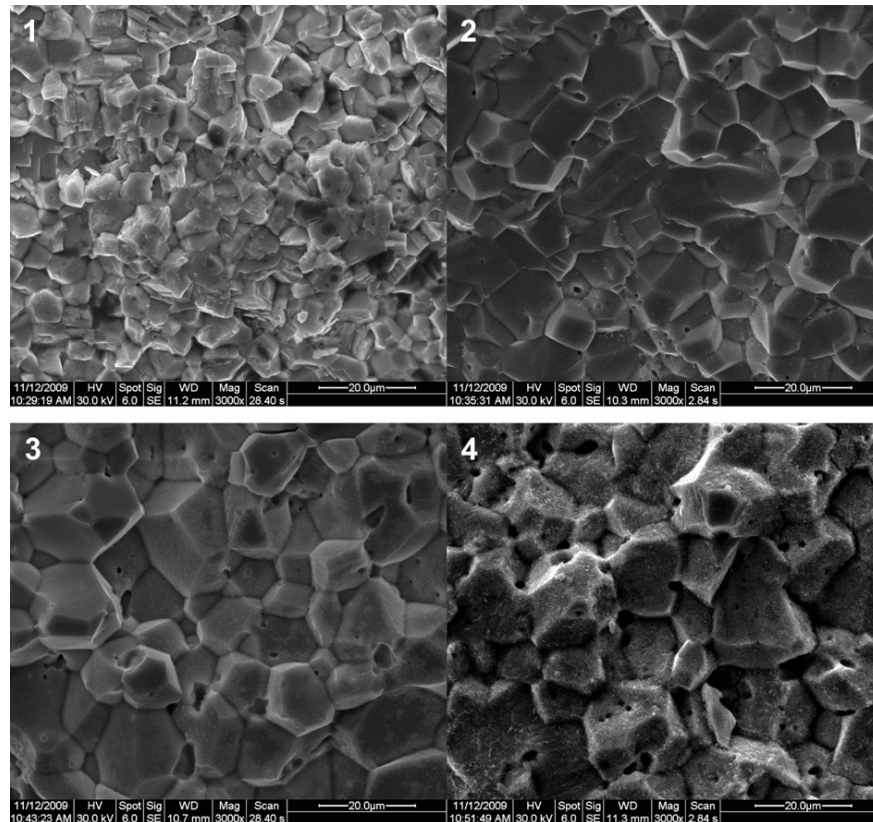


Fig. 3 – The cross-sectional views of different pellets sintered at 1450 °C for 5 h in air after all conductivity measurements. (1) $\text{BaIn}_{0.3}\text{Ce}_{0.7}\text{O}_{3-\delta}$ (2) $\text{BaIn}_{0.2}\text{Y}_{0.1}\text{Ce}_{0.7}\text{O}_{3-\delta}$ (3) $\text{BaIn}_{0.1}\text{Y}_{0.2}\text{Ce}_{0.7}\text{O}_{3-\delta}$ (4) $\text{BaY}_{0.3}\text{Ce}_{0.7}\text{O}_{3-\delta}$.

3.3. Chemical stability

To investigate the chemical stability of the $\text{BaIn}_{0.3-x}\text{Y}_x\text{Ce}_{0.7}\text{O}_{3-\delta}$ ($x = 0, 0.1, 0.2, 0.3$), the BIYC disks were exposed to wet 3 vol% CO_2 (air as the balance gas, 3 vol% H_2O) with a flow rate of 40 mL min^{-1} at 700 °C for 24 h. The formation of BaCO_3 and CeO_2 can be observed in the XRD patterns shown in Fig. 4. The number and intensity of the impurity peaks were observed to increase with the increase in Y doping content, suggesting that the tolerance to CO_2 decreases with Y doping for $\text{BaIn}_{0.3-x}\text{Y}_x\text{Ce}_{0.7}\text{O}_{3-\delta}$ ($x = 0, 0.1, 0.2, 0.3$) ceramics. For example, although the main perovskite structure phase of BIYC remains, the reaction between $\text{BaY}_{0.3}\text{Ce}_{0.7}\text{O}_{3-\delta}$ and wet CO_2 is more severe than that for $\text{BaIn}_{0.3}\text{Ce}_{0.7}\text{O}_{3-\delta}$. The intensity of the impurity peaks in the XRD patterns of $\text{BaIn}_{0.3}\text{Ce}_{0.7}\text{O}_{3-\delta}$ is negligible compared to that of the characteristic perovskite peaks, which is consistent with the results reported by Bi et al. [19].

3.4. Conductivity study

Shown in Fig. 5 are the conductivities of the $\text{BaIn}_{0.3-x}\text{Y}_x\text{Ce}_{0.7}\text{O}_{3-\delta}$ ($x = 0, 0.1, 0.2, 0.3$) samples in different atmospheres in the temperature range of $550\text{--}800 \text{ °C}$. Among all the samples examined, $\text{BaY}_{0.3}\text{Ce}_{0.7}\text{O}_{3-\delta}$ shows the highest conductivities: 3.36×10^{-2} , 3.5×10^{-2} , 2.40×10^{-2} and $2.71 \times 10^{-2} \text{ S cm}^{-1}$ in dry

air, wet air, wet nitrogen and wet hydrogen at 800 °C , respectively. However, the chemical stability of $\text{BaY}_{0.3}\text{Ce}_{0.7}\text{O}_{3-\delta}$ is quite unsatisfactory according to XRD study shown above. $\text{BaIn}_{0.1}\text{Y}_{0.2}\text{Ce}_{0.7}\text{O}_{3-\delta}$ shows an acceptable stability and relatively high conductivity: 1.27×10^{-2} , 1.33×10^{-2} , 8.52×10^{-3} and $8.7 \times 10^{-3} \text{ S cm}^{-1}$ in dry air, wet air, wet nitrogen and wet hydrogen at 800 °C , respectively. At a given operating temperature, the conductivities of BIYC samples increase with the amount of Y

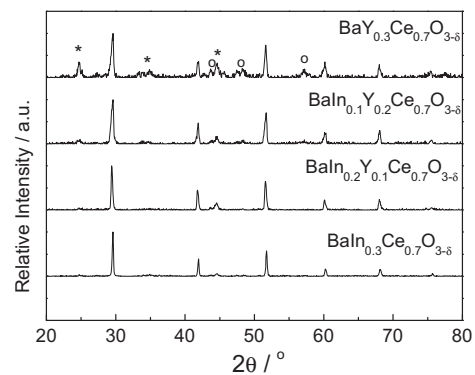


Fig. 4 – XRD patterns of $\text{BaIn}_{0.3-x}\text{Y}_x\text{Ce}_{0.7}\text{O}_{3-\delta}$ ($x = 0, 0.1, 0.2, 0.3$) disks measured on the surfaces after exposure to wet 3% CO_2 with air as the balance gas at 700 °C for 24 h. *: BaCO_3 , o: CeO_2 .

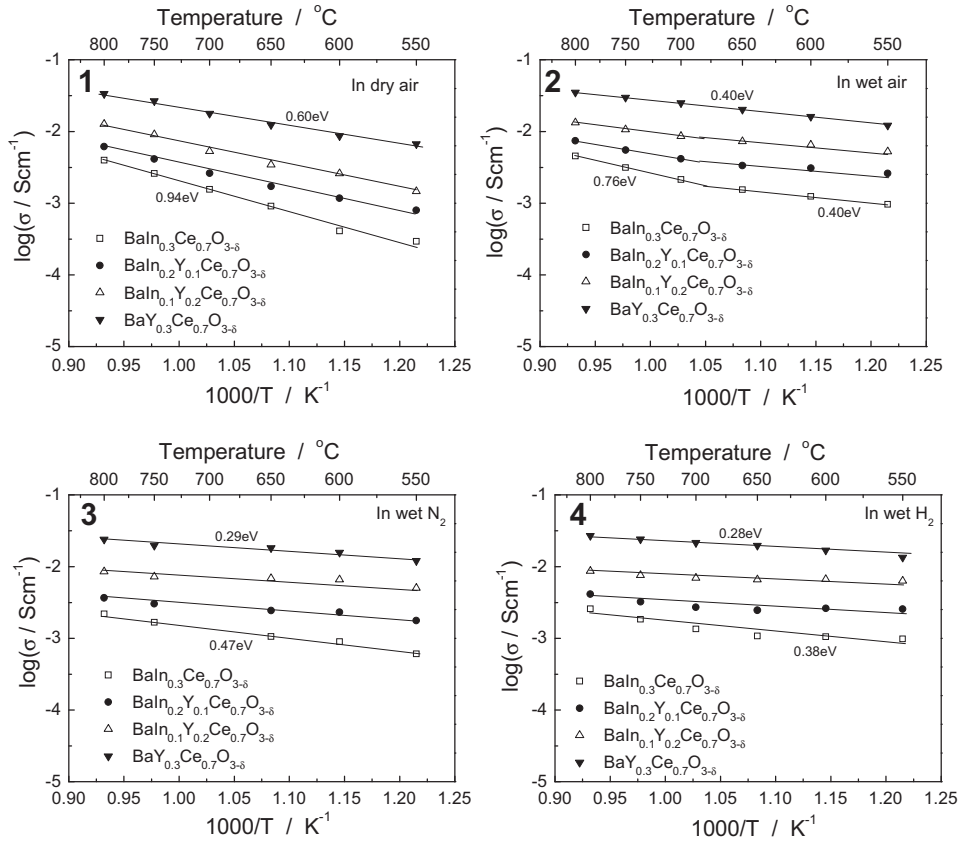


Fig. 5 – Effect of temperature on the conductivity of the $\text{BaIn}_{0.3-x}\text{Y}_x\text{Ce}_{0.7}\text{O}_{3-\delta}$ ($x = 0, 0.1, 0.2, 0.3$) samples in dry air (1), wet air (2), wet nitrogen (3) and wet hydrogen (4).

doping. This result can be partially predicted by the SEM observations shown in Fig. 2 due to the increasing number of grain boundaries in low concentration of the Y doping. From the change of slope coefficient shown in Fig. 5(1), (3) and (4), it indicates that the activation energies for total conductivity of the $\text{BaIn}_{0.3-x}\text{Y}_x\text{Ce}_{0.7}\text{O}_{3-\delta}$ system in dry air, wet N_2 and wet H_2 decrease with the increase of the Y content. For example, in dry air (Fig. 5(1)) the activation energies are 0.60 eV and 0.94 eV for $\text{BaY}_{0.3}\text{Ce}_{0.7}\text{O}_{3-\delta}$ and $\text{BaIn}_{0.3}\text{Ce}_{0.7}\text{O}_{3-\delta}$, respectively. Since air contains approximately 20 vol% oxygen, oxygen-ion conduction is expected to be dominant for the BIYC samples. However, since doped BaCeO_3 is oxygen deficient, in wet atmosphere, the presence of reaction (2) could lead to mixed protonic and electronic conductivity [13,26,27], resulting in relatively lower activation energies ranging from 0.28 eV to 0.47 eV when the BIYC samples are tested in wet nitrogen and wet hydrogen atmospheres. The conductivities of all samples in wet hydrogen (Fig. 5(4)) are found to be lower than those in dry (Fig. 5(1)) and wet (Fig. 5(2)) air, probably due to the presence of oxygen-ion and hole conductivity in air since the hole conductivity depends on the oxygen vacancy concentration introduced through doping with trivalent ions and oxygen partial pressure of the testing environment [28]. Meanwhile, slope changes in Fig. 5(2) for the In-doped samples in the temperature regions of 650–700 °C

could be related to a change of the conduction mechanism when water vapor and air are present, as derived from the change of the effective charge carriers' concentration [29,30]. As shown in Fig. 5(2), the activation energy of $\text{BaIn}_{0.3}\text{Ce}_{0.7}\text{O}_{3-\delta}$ under wet air increased from 0.40 eV to 0.76 eV, indicating that the predominant conduction phenomena changed from proton conduction at low temperatures to oxygen-ion conduction at high temperatures.

4. Conclusions

In summary, $\text{BaIn}_{0.3-x}\text{Y}_x\text{Ce}_{0.7}\text{O}_{3-\delta}$ ($x = 0, 0.1, 0.2, 0.3$) powders have been successfully synthesized by a modified Pechini method. An increase in the yttrium content in $\text{BaIn}_{0.3}\text{Ce}_{0.7}\text{O}_{3-\delta}$ resulted in enhanced conductivity in both dry air and wet hydrogen, and the highest conductivity was observed for $x = 0.3$ ($3.5 \times 10^{-2} \text{ S cm}^{-1}$ in wet air at 800 °C). The sinterability of $\text{BaIn}_{0.3-x}\text{Y}_x\text{Ce}_{0.7}\text{O}_{3-\delta}$ ($x = 0, 0.1, 0.2, 0.3$) decreased with the increase in Y doping content. However, tolerance to wet CO_2 for $\text{BaIn}_{0.3-x}\text{Y}_x\text{Ce}_{0.7}\text{O}_{3-\delta}$ samples decreased with the increase of the amount of Y doping. Among all the compositions, $\text{BaIn}_{0.1}\text{Y}_{0.2}\text{Ce}_{0.7}\text{O}_{3-\delta}$ has relatively high conductivity as well as acceptable stability in wet CO_2 atmosphere.

Acknowledgements

The financial support of the Department of Energy Nuclear Energy University Program (NEUP) (award no. 09-510) and the South Carolina Universities Research and Education Foundation (award no. 09-155) is acknowledged gratefully.

REFERENCES

- [1] Minh NQ. Ceramic fuel cells. *J Am Ceram Soc* 1993;76(3):563–88.
- [2] Bonanos N, Ellis B, Mahmood MN. Construction and operation of fuel cells based on the solid electrolyte BaCeO₃:Gd. *Solid State Ionics* 1991;44:305–11.
- [3] Nowick AS, Du Y. High-temperature protonic conductors with perovskite-related structures. *Solid State Ionics* 1995;77:137–46.
- [4] Bonanos N, Knight KS, Ellis B. Perovskite solid electrolytes: structure, transport properties and fuel cell applications. *Solid State Ionics* 1995;79:161–70.
- [5] Virkar AN, Maiti HS. Oxygen ion conduction in pure and yttria-doped barium cerate. *J Power Sources* 1985;14:295–303.
- [6] Künstler K, Lang HJ, Maiwald A, Tomandle G. Synthesis, structure and electrochemical properties of In-doped BaCeO₃. *Solid State Ionics* 1998;107:221–9.
- [7] Chen FL, Toft Sørensen O, Meng GY, Peng DK. Preparation of Nd-doped BaCeO₃ proton-conducting ceramic and its electrical properties in different atmospheres. *J Eur Ceram Soc* 1998;18:1389–95.
- [8] Wu ZL, Liu ML. Stability of BaCe_{0.8}Gd_{0.2}O₃ in a H₂O-containing atmosphere at intermediate temperatures. *J Electrochem Soc* 1997;144(6):2170–5.
- [9] Peng RR, Wu Y, Yang LZ, Mao ZQ. Electrochemical properties of intermediate-temperature SOFCs based on proton conducting Sm-doped BaCeO₃ electrolyte thin film. *Solid State Ionics* 2006;177:389–93.
- [10] Yamaguchi S, Yamada N. Thermal lattice expansion behavior of Yb-doped BaCeO₃. *Solid State Ionics* 2003;162:163:23–9.
- [11] Wang JX, Li LP, Campbell BJ, Lv Z, Ji Y, Xue YF, et al. Structure, thermal expansion and transport properties of BaCe_{1-x}Eu_xO_{3-δ} oxides. *Mater Chem Phys* 2004;86:150–5.
- [12] Kreuer KD. Proton-conducting oxides. *Annu Rev Mater Res* 2003;33:333–59.
- [13] Iwahara H. Proton conducting ceramics and their applications. *Solid State Ionics* 1996;86–88:9–15.
- [14] Coors WG. Steam reforming and water–gas shift by steam permeation in a protonic ceramic fuel cell. *J Electrochem Soc* 2004;151(7):A994–7.
- [15] Iwahara H, Asakura Y, Katahira K, Tanaka M. Prospect of hydrogen technology using proton-conducting ceramics. *Solid State Ionics* 2004;168:299–310.
- [16] Haile SM, Staneff G, Ryu KH. Non-stoichiometry, grain boundary transport and chemical stability of proton conducting perovskites. *J Mater Sci* 2001;36:1149–60.
- [17] Zhang C, Zhao H, Xu N, Li X, Chen N. Influence of ZnO addition on the properties of high temperature proton conductor Ba_{1.03}Ce_{0.5}Zr_{0.4}Y_{0.1}O_{3-δ} synthesized via citrate–nitrate method. *Int J Hydrogen Energy* 2009;34:2739–46.
- [18] Matskevich NI. Enthalpy of formation of BaCe_{0.9}In_{0.1}O_{3-δ}. *J Therm Anal Calorim* 2007;90:955–8.
- [19] Bi L, Zhang SQ, Zhang L, Tao ZT, Wang HQ, Liu W. Indium as an ideal functional dopant for a proton-conducting solid oxide fuel cell. *Int J Hydrogen Energy* 2009;34:2421–5.
- [20] Matsumoto H, Kawasaki Y, Ito N, Enoki M, Ishihara T. Relation between electrical conductivity and chemical stability of BaCeO₃-based proton conductors with different trivalent dopants. *Electrochem Solid State Lett* 2007;10(4):B77–80.
- [21] Bi L, Zhang SQ, Fang SM, Tao ZT, Peng RR, Liu W. A novel anode supported BaCe_{0.7}Ta_{0.1}Y_{0.2}O_{3-δ} electrolyte membrane for proton-conducting solid oxide fuel cell. *Electrochem Commun* 2008;10:1598–601.
- [22] Xie K, Yan RQ, Liu XQ. Stable BaCe_{0.7}Ti_{0.1}Y_{0.2}O_{3-δ} proton conductor for solid oxide fuel cells. *J Alloys Compd* 2009;479:L40–2.
- [23] Xie K, Yan RQ, Liu XQ. The chemical stability and conductivity of BaCe_{0.9-x}Y_xSn_{0.1}O_{3-δ} solid proton conductor for SOFC. *J Alloys Compd* 2009;479:L36–9.
- [24] Giannici F, Longo A, Balerna A, Kreuer KD, Martorana A. Indium doping in barium cerate: the relation between local symmetry and formation and mobility of protonic defects. *Chem Mater* 2007;19:5714–20.
- [25] Ding D, Li L, Feng K, Liu Z, Xia C. High performance Ni–Sm₂O₃ cermet anodes for intermediate-temperature solid oxide fuel cells. *J Power Sources* 2009;187:400–2.
- [26] Kosacki I, Tuller HL. Mixed conductivity in SrCe_{0.95}Yb_{0.05}O₃ protonic conductors. *Solid State Ionics* 1995;80:223–9.
- [27] He T, Kreuer KD, Baikov YM, Maier J. Impedance spectroscopic study of thermodynamics and kinetics of a Gd-doped BaCeO₃ single crystal. *Solid State Ionics* 1997;95:301–8.
- [28] Shimura T, Tanaka H, Matsumoto H, Yogo T. Influence of the transition-metal doping on conductivity of a BaCeO₃-based protonic conductor. *Solid State Ionics* 2005;176:2945–50.
- [29] Gorbova E, Maragou V, Medvedev D, Demin A, Tsiakaras P. Investigation of the protonic conduction in Sm doped BaCeO₃. *J Power Sources* 2008;182(2):207–13.
- [30] Frade JR. Theoretical behaviour of concentration cells based on ABO₃ perovskite materials with protonic and oxygen ion conduction. *Solid State Ionics* 1995;78:87–97.